

Mechanochemical Synthesis of Sn(II) and Sn(IV) Iodide Perovskites and Study of Their Structural, Chemical, Thermal, Optical and Electrical Properties

Yousra El Ajjouri, Federico Locardi, María C. Gélvez-Rueda, Mirko Prato, Michele Sessolo, Maurizio Ferretti, Ferdinand C. Grozema, Francisco Palazon* and Henk J. Bolink

Y. El Ajjouri, Dr. M. Sessolo, Dr. F. Palazon, Prof. H. J. Bolink
Instituto de Ciencia Molecular, ICMol, Universidad de Valencia
C/ Catedrático J. Beltrán 2, 46980 Paterna, Spain
E-mail: Francisco.palazon@uv.es

Dr. F. Locardi, Prof. M. Ferretti
Dipartimento di Chimica e Chimica Industriale, Università degli Studi di Genova
Via Dodecaneso 31, 16146 Genova, Italy

Dr. F. Locardi, Dr. F. Palazon
Nanochemistry Department, Istituto Italiano di Tecnologia
Via Morego 30, 16163 Genova, Italy

M. C. Gélvez-Rueda, Dr. F. C. Grozema
Optoelectronic Materials Section, Department of Chemical Engineering, Delft University of Technology
Van der Maasweg 9, 2629 HZ Delft, The Netherlands

Dr. M. Prato,
Materials Characterization Facility, Istituto Italiano di Tecnologia
Via Morego 30, 16163 Genova, Italy

Keywords: perovskites, mechanochemistry, solid-state, tin, low-bandgap

Phase-pure CsSnI_3 , FASnI_3 , $\text{Cs}(\text{PbSn})\text{I}_3$, $\text{FA}(\text{PbSn})\text{I}_3$ perovskites (FA = formamidinium = $\text{HC}(\text{NH}_2)_2^+$) as well as the analogous so-called “vacancy-ordered double perovskites” Cs_2SnI_6 and FA_2SnI_6 were mechanochemically synthesized. The addition of SnF_2 was found to be crucial for the synthesis of Cs-containing perovskites but unnecessary for hybrid ones. All compounds show an absorption onset in the near-IR region, which makes them especially relevant for photovoltaic applications. The addition of Pb(II) and SnF_2 is crucial to improve the electronic properties in 3D Sn(II)-based perovskites, in particular their charge carriers mobility ($\sim 0.2 \text{ cm}^2/\text{V}\cdot\text{s}$) which is enhanced upon reduction of the dark carrier conductivity. Stokes-shifted photoluminescence is observed on dry powders of Sn(II)-based perovskites, which

makes these materials promising for light-emitting and sensing applications. Thermal stability of all compounds has been examined, revealing no significant degradation up to at least 200 °C. This meets the requirements for standard operation conditions of most optoelectronic devices and is potentially compatible with thermal vacuum deposition of polycrystalline thin films.

1. Introduction

Lead iodide perovskites have shown excellent photovoltaic (PV) as well as electroluminescent properties.^[1,2] In part due to the toxicity of Pb²⁺ ions, other metal halide perovskites are being investigated. Divalent tin is the most straightforward alternative to lead, considering their similar electronic configuration (group 14) and similar ionic radiuses.^[3–34] Furthermore, mixed Sn-Pb iodide perovskites possess a lower bandgap than pure Pb and Sn ones, with applications in both single junction and tandem solar cells.^[35] One problem that arises with the use of Sn(II) is that it may be easily oxidized to Sn(IV). Two workarounds exist to this problem: (i) limiting the oxidation by using additives such as SnF₂,^[8,11,12,33,36] or (ii) exploring the properties of Sn(IV)-based materials.^[37–48] A₂B(IV)X₆ compounds can be seen as a similar structure to the AB(II)X₃ perovskite where every other BX₆ octahedra is removed, and B is in +4 oxidation state to ensure charge neutrality (see Scheme 1).

These compounds are sometimes referred to as *vacancy-ordered double perovskites*, where the B-“vacancies” are described as *virtual cations*, also explaining why the stoichiometry of A₂BX₆ is often written as 2-□-1-6. Cs₂SnI₆ has been shown to be a degradation product of CsSnI₃ upon air-exposure.^[46] Although this compound can be seen as a zero-dimensional structure due to the fact that adjacent SnI₆ octahedra do not share any corners, their vicinity and consequent orbital overlap results in interesting optoelectronic properties for PV.^[46] Mechanochemical synthesis *via* ball-milling or other techniques (*e.g.*, hand grinding) provides an ideal platform to form a wide variety of perovskites in stoichiometric and solvent-free conditions.^[49,50,50–70]

Additionally, these compounds may later be used for thin film deposition by single-source thermal evaporation.^[52] The high number of recent publications indicate that mechanochemical synthesis is starting to be a common practice in a few research groups focusing on halide perovskites and related compounds, and we foresee that it will be a widespread approach in the near future. Surprisingly, given the interest on tin perovskites, we could only find two publications focusing on mechanochemical synthesis of such compounds. The first one is the seminal work of Stoumpos et al.^[71] where mechanochemical synthesis (grinding by hand with mortar and pestle) was found to yield non-pure perovskites with considerable amounts of unreacted precursors. The second reference is a recent work from Sasaki et al.^[59] where several 3D pure-tin mixed iodide-bromide perovskites were synthesized. To the best of our knowledge, no reports either on mixed Sn-Pb (especially relevant for low bandgap applications as previously discussed) or on 0D iodide perovskites by mechanochemistry exist. Also, the only report of 3D iodide perovskites made by mechanochemical synthesis that we are aware of^[59] does not provide thermal stability or electrical conductivity characterization.

Hereafter, we have used ball-milling to synthesize the pure Sn and mixed Sn-Pb iodide perovskites CsSnI₃, FASnI₃, Cs(PbSn)I₃, and FA(PbSn)I₃ as well as the Sn(IV)-based vacancy-ordered perovskites Cs₂SnI₆ and FA₂SnI₆ (FA = formamidinium = HC(NH₂)₂⁺). The influence of SnF₂ as additive in the synthesis is also investigated. The elemental, chemical and structural characteristics of the as-prepared compounds are investigated by X-ray diffraction (XRD) and X-ray photoelectron spectroscopy (XPS). Furthermore, the thermal stability is studied by means of differential thermal analysis and thermogravimetry (DTA/TG). The energy level diagram is estimated from optical characterization and ultraviolet photoelectron spectroscopy (UPS). In addition, the charge carrier mobility and lifetime of 3D Sn(II)-based perovskite and 0D Sn(IV)-based structure were investigated by time-resolved microwave conductivity (TRMC), revealing that the effective mobility is two orders of magnitude larger for 3D Sn(II)-based perovskites as compared to 0D Sn(IV)-based structures. These measurements show that the electronic

properties of fully-inorganic Sn(II)-based perovskites are improved during synthesis by Pb-mixing and addition of SnF₂, which decreases the charge carrier conductivity caused by oxidation to Sn(IV).

2. Results and Discussion

Sn(II)- and Sn(IV)-based compounds were synthesized by dry ball-milling of stoichiometric mixtures of the different precursors (see experimental section for details). Figure 1 shows the XRD characterization of all metal iodide perovskites.

The X-ray diffractograms of CsSnI₃, FASnI₃, Cs₂SnI₆, and FA₂SnI₆ match very well with the corresponding reference bulk patterns. The mixed tin-lead compounds Cs(SnPb)I₃ and FA(SnPb)I₃ have XRD signals comparable to the pure tin compounds albeit slightly shifted to lower angles, as expected from a partial replacement of tin with a bigger cation such as lead. Accordingly, we also observe a shift to lower diffraction angles in FA-based compounds compared to Cs-based ones. These differences are more clearly observed in Figure S2, which shows the three more relevant regions of each diffractogram. The high phase purity and match with reference XRD patterns highlight the potential of mechanochemical synthesis to obtain high quality materials. As noted in the legend of Figure 1, CsSnI₃ and Cs(PbSn)I₃ were formed in the presence of SnF₂. This additive was found to be crucial in the synthesis of CsSnI₃ (but not in the synthesis of FASnI₃) to avoid the formation of SnI₄, as revealed by thermal analyses (Figure 2, and Figures S3-S5). In particular, when comparing the DTA signal of CsSnI₃ synthesized with and without SnF₂ (Figure S3), an endothermic peak around 160 °C, ascribed to the melting of SnI₄, is visible only in the case where no SnF₂ is added. This peak is also absent in the case of FASnI₃ even without additive (Figure 2).

Besides the effect of SnF₂, all the samples were analyzed through DTA/TG to investigate their thermal stability (Fig. 2). CsSnI₃ is stable up to 450 °C, temperature at which it melts with the

subsequent vaporization of SnI₂ and CsI.^[14] A very similar behavior was recorded for Cs(SnPb)I₃ (Fig. S4). Cs₂SnI₆ seems less stable, decomposing at ~320 °C due to SnI₄ (b.p. ~ 350 °C) which is more volatile than SnI₂ (b.p. ~ 700 °C). Indeed, the TG variation, equal to 53.6 % and 47.0 % in the first and second step, respectively, are consistent with the loss of SnI₄ and CsI (whose melting point is reported in the DTA curve at 627 °C). FASnI₃ and FA(SnPb)I₃ have considerable lower stability respect to the Cs-based counterparts because of the organic cation, which mainly drives the decomposition mechanism.^[72] Interestingly, FA₂SnI₆ is slightly more stable with respect to FASnI₃ and FA(SnPb)I₃, with the initial weight loss starting around 250 °C instead of 200 °C. This might be due to a stronger interaction between FA molecules in FA₂SnI₆. However, the weight loss is much faster in this Sn(IV) compound, being completely vaporized at 400 °C, consistent with the reaction: FA₂SnI₆ → 2 FAI + SnI₄. Similarly, the decomposition mechanism for FASnI₃ and FA(SnPb)I₃ could be summarized, respectively, as FASnI₃ → FAI + SnI₂ and FA(SnPb)I₃ → FAI + ½ SnI₂ + ½ PbI₂.^[73] However, their TG and DTA curves evidence a more complex mechanism involving the formation of several intermediates. The last weight losses in TG curves of FASnI₃ and FA(SnPb)I₃ start at ~ 500 °C, temperature at which SnI₂ is released, as also observed in the inorganic Cs-based counterparts (Figure S4). This further confirms that Sn remains in +2 oxidation state in these hybrid perovskites without addition of SnF₂.

All Sn(II) and Sn(IV) perovskites were further analyzed by high-resolution XPS, in order to gather quantitative information on their chemical composition (XPS spectra of all compounds are shown in Figure 3 and atomic percentages of relevant elements are given in Table 1).

Carbon C 1s spectra of all samples show a peak at low binding energy (BE) which is ascribed to C-C bonds of adventitious carbon originating from exposure to organic volatile compounds in air. This peak is fixed to BE = 284.5 eV for energy calibration, as standard practice. FA-based samples show a second peak at BE = 287.9 +/- 0.2 eV assigned to the carbon atom in

formamidinium cations. Although not shown in Figure 3, CsSnI₃ and Cs(SnPb)I₃ samples exhibit an additional peak at BE = 684.0 eV corresponding to the F 1s orbital from SnF₂ (see Figure S6). Quantitative elemental analysis can be derived from these high-resolution spectra, after correcting for SnF₂ contribution and considering only the highest energy component of C 1s. Atomic percentages of all relevant elements are given in Table 1.

Several observations can be made from Table 1. First of all, FA₂SnI₆ seems highly degraded as only a very low amount of tin is detected. This suggests that this compound is severely affected by X-ray radiation and ultrahigh vacuum, leading most likely to the formation and subsequent loss of SnI₄. For all the other compounds we note that the A:B ratios (where A is either Cs or FA and B is either Sn or SnPb) are very close to the expected 1:1 or 2:1 ratios, further confirming the material purity already observed by XRD. The same is true for the Sn:Pb ratios, which are close to 1:1 in both mixed tin-lead perovskites. The C:N ratios in FA-based samples are close to the expected 1:2 ratio for FA cations, confirming the assignment of the high-BE component of C 1s spectra to FA and, importantly, suggesting that FA is not degraded during mechanochemical synthesis. This is not obvious *a priori*, as FAI is known to give different degradation byproducts, such as HCN or others, which could be volatile and hence alter the C:N ratio in the sample.^[74] Nonetheless, we note that in all samples the measured iodine concentration is lower than expected. In regards to this, it should be noted that we also observe oxygen (see Figure S7), which is likely due to oxidation upon air exposure prior to analysis. Indeed, although the synthesis is carried out under nitrogen (see experimental section for details), the samples are exposed to air for a short time before characterization. As photoelectron spectroscopies are surface-sensitive techniques (depth of analysis is typically few nanometers), even a small superficial oxidation will have a high impact on XPS results. In other words, it is unlikely that a significant formation of SnO_x affects the bulk of the perovskites here, as these species do not appear in the XRD signal (Figure 1). Furthermore, based on literature, the formation of significant SnO_x in the bulk from air exposure is a process that typically takes

several days or weeks.^[46] A closer look at XPS spectra (Figure 3) allows to further discuss the oxidation states and chemical environments of the different elements in all samples. In the case of Cs-based samples, the Cs 3d spectra show a doublet with Cs 3d_{5/2} peak located at BE = 724.0 +/- 0.3 eV as well as I 3d spectra with I 3d_{5/2} at BE = 618.7 eV +/- 0.2 eV. These values are consistent with Cs(+1) and I(-1) oxidation states expected for inorganic iodide perovskites.^[75] The Sn 3d spectra of CsSnI₃ and Cs(SnPb)I₃ show two clear components (two doublets) ascribed to the addition of SnF₂ in these samples, while Cs₂SnI₆ shows only one component, as expected. Comparing the BE values of Sn(II) and Sn(IV) reported in literature, it seems unlikely to easily distinguish them, as these values largely overlap.^[76] In the case of Cs(SnPb)I₃ we note that Pb 4f spectra are asymmetric with a low-BE component whose origin could not be clearly elucidated. Importantly, no metallic lead (or tin) was observed in any of the samples (the Sn 3d and Pb 4f peak positions for metallic tin and lead are indicated by dashed lines in Figure 2), which could otherwise have a detrimental effect on the perovskite optoelectronic properties.^[77-79] In the case of FA-based samples, the peak at BE = 287.9 +/- 0.2 eV is assigned to the carbon atom of FA cations. Accordingly, the N 1s peak is at BE = 400.2 +/- 0.1 eV, corresponding to the N atoms of FA. Interestingly, FASnI₃ sample shows a second peak at lower BE which may be ascribed to deprotonated amines in FA (noted in the graph as C-NH₂⁰).^[80,81] Here, the deprotonation of FA is concomitant to the formation of different iodine species, as evidenced by the I 3d spectra, which only in the case of FASnI₃ shows two different components. It is possible that a partial proton transfer from FA to I⁻ occurs. Nonetheless, the complexity of iodine chemistry in hybrid perovskites complicate the identification of the exact species formed here.^[82] Sn 3d spectra of the three FA-based compounds show a main Sn 3d_{5/2} peak centered at BE = 487.1 +/- 0.1 eV, consistent both with Sn(II) and Sn(IV) iodide perovskites.^[30] A small component at lower BE appears in the Sn 3d spectrum in the case of FA(SnPb)I₃ sample, somehow similar to the lead signal in Cs(SnPb)I₃. This low BE component might be due to oxidation as previously discussed. In summary, aside from FA₂SnI₆ that is degraded under

characterization, XPS spectra confirm overall the formation of the entire series of compounds, with signals that match with the expected spectra of the different perovskites (and the corresponding signal for SnF_2 in the CsSnI_3 and $\text{Cs}(\text{SnPb})\text{I}_3$ samples).

Optical characterization (diffuse reflectance and photoluminescence) as well as ultraviolet photoelectron spectroscopy (UPS) were performed to estimate the energetic positions of the valence band, Fermi level and conduction band of these materials (Figure 4).

All compounds have an absorption onset in the near-infrared (NIR) region, suited for single junction solar cells as well as rear absorber in perovskite-perovskite tandem devices. All Sn(II)-based compounds have clear Stokes-shifted photoluminescence at room temperature (Figure 4), which make them potentially interesting also for near-infrared light-emitting diodes. The UPS secondary electron cut-off (Figure 4, middle column) and onset (right column) allow us to determine the work function and the energy difference between the Fermi level and the top of the valence band, respectively. Combining this information, we are able to estimate the characteristic energy levels as presented at the bottom of Figure 4. The addition of lead to Sn(II)-based perovskites results in deeper energy levels as compared to the pure-tin counterparts, which is consistent with the literature.^[83] Furthermore, a red-shift in PL is clearly observed from pure-tin FASnI_3 to mixed tin-lead $\text{FA}(\text{SnPb})\text{I}_3$. Such behavior has also been noted by others, where mixed tin-lead perovskites were found to have a lower bandgap than both pure-tin and pure-lead compositions.^[84] Interestingly we do not observe this phenomenon in inorganic Cs-based perovskites. The apparent p-type doping in FASnI_3 may be ascribed to a partial oxidation of Sn(II) to Sn(IV).^[85] On the other hand, mixed $\text{FA}(\text{SnPb})\text{I}_3$ seems to be rather n-type. The origin of this effect is not fully elucidated. However, we already noted in the discussion of XPS data (Figure 3, blue spectra) that tin appeared to be slightly reduced, which might explain the n-type character observed here. Again, these effects do not seem to be significant for inorganic Cs-based compounds, as both appear rather intrinsic semiconductors. It must be noted though

that these perovskites were formed with addition of SnF₂. We therefore infer that SnF₂ helps maintaining the intrinsic nature of the semiconductor by preventing oxidation of tin. For Sn(IV) compounds, we clearly see a difference from the valence band maximum to the Fermi level (UPS onset, right column) of 1.5 eV, close to the reported bandgap for the same material.^[86] Unfortunately, we cannot determine the optical bandgap, due to the smooth absorption onset and lack of photoluminescence. As it cannot be lower than 1.5 eV, we take this as the bandgap (it seems a reasonable assumption considering that the sample is clearly black; see Figure S8). These observations mean that these materials are heavily n-doped. Again, this conclusion is in agreement with literature, where Cs₂SnI₆ has been reported by several groups to be intrinsically n-type.^[45]

Eventually, we studied the mobility and lifetime of charge carriers by pulse-radiolysis time-resolved microwave conductivity (PR-TRMC). In this technique, materials are ionized with a high energy electron pulse and, subsequently, the change in conductivity is probed with GHz microwaves. If irradiation leads to mobile charge carriers, these will absorb part of the microwave power, decreasing the microwave power reflected by the cell. This decrease in microwave power is directly related to the change in conductivity and ultimately to the mobility of charge carriers.^[87] We note that in most samples, measurements were not possible due to high or even complete absorption of the microwaves without irradiation. This is indicative of a considerable dark conductivity that hinders the detection of changes in conductivity upon irradiation. This behaviour matches with the UPS measurements, where we observe that most samples are doped either with a p-type character, most likely caused by oxidation of Sn²⁺ to Sn⁴⁺, or a n-type character. It has been shown in literature that presence of low concentrations of dark charge carriers has a strong detrimental effect on the electronic properties.^[8,11,12,33,36] In fact, we are able to observe change of reflection (not quantifiable) that is very short-lived (<5ns), which indicates that the generated charge carriers recombine or are trapped within the time resolution of the PR-TRMC experiment (see Figure S9). Nevertheless, we were able to obtain

meaningful results on two compounds: a 3D Sn(II)-based compound ($\text{Cs}(\text{SnPb})\text{I}_3$) and a 0D Sn(IV)-based compound (FA_2SnI_6), which are hereafter simply referred to as 3D and 0D samples (Figure 5a). The fact that we can measure these samples matches with the UPS measurements, where $\text{Cs}(\text{SnPb})\text{I}_3$ seems to be an intrinsic semiconductor. This intrinsic character is most likely achieved during synthesis. Where decreasing tin content with lead and adding SnF_2 suppresses Sn^{2+} oxidation to Sn^{4+} and as a result decreases the concentration of dark charge carriers. This is also in line with reported improved stabilities of tin based perovskites when also lead cations are present.^[88]

As can be seen in Figure 5a, the 3D sample shows a charge carrier mobility is 2 orders of magnitude higher compared to the 0D sample (0.2 and 0.004 cm^2/Vs , respectively). This is not surprising if we consider that the higher dimensionality of the 3D sample leads to a higher overlap of molecular orbitals. In both cases, the mobility was not found to significantly change when cooling from RT to 173 K. This indicates that the charge carrier mobility is not dominated by lattice scattering, but may be controlled by defects. The mobility of the 3D sample is of the same order of magnitude as for 3D lead-based perovskite samples prepared without the use of solvents,^[89] while it is one to two orders of magnitude lower than 3D lead-based perovskites prepared by precipitation or single crystals, respectively.^[89,90] This points out that dry mechanochemical synthesis as performed here might lead to a higher density of defects as opposed to solution-processing. Nonetheless, we believe that the synthesis may be optimized, for example by reducing the grinding time, which in this case was 5 hours. Such a long time is probably unnecessary to yield phase pure perovskites, and reducing it will likely limit detrimental effects of prolonged grinding (*i.e.* tin oxidation). The time-resolved conductivity (Figure 5b) of the 3D sample shows a fast-initial decay followed by a long-tail that does not decay to zero, even at very long times. Also, the maximum change in conductivity increases with the initial concentration of charge carriers (increase pulse length; see Figure S10). This behavior is similar to the observed for 3D MAPbX_3 samples,^[89] and is attributed to second order

recombination with a limited concentration of trap states.^[89] The fast-initial decay is caused by trapping of one of the charges and the long tail signal comes from the remaining free charges.^[89,90] As for the mobility, the carrier lifetime seems almost unaffected by temperature (see Figure S11), indicating that the decay is still dominated by the recombination with a similar concentrations of the trap states as at room temperature. In the case of the 0D sample, the conductivity signal is very low and decays in less than 50 ns (Figure 5b). However, we observe a slight conductivity increase at low temperatures which may be related to less thermal vibration of the lattice (see Figure S12).

3. Conclusion

In conclusion we have been able to synthesize hybrid and inorganic pure-tin and mixed tin-lead iodide perovskites and vacancy ordered perovskites with excellent phase purity as revealed by XRD. Detailed thermal stability studies were carried out revealing that all compounds are stable up to 200 °C, which is compatible with common operational conditions in optoelectronic devices. Inorganic perovskites based on Sn(II) were found to be stable beyond 400 °C, making them good candidates for single source thermal deposition in thin films. Indeed, these compounds show a narrow bandgap suited for photovoltaics and near-IR LEDs. The charge carrier mobility was found to be rather low which could be due to oxidation during the long ball-milling mechanochemical synthesis. However, we demonstrated that the dark carrier conductivity in inorganic 3D Sn(II)-based compounds can be improved by addition of Pb(II) and/or SnF₂ during synthesis. Ongoing work is focused on optimizing the preparation conditions, especially reducing the grinding time to an ideal duration that will ensure a complete synthesis while avoiding possible detrimental effects.

Supporting Information

Supporting Information is available from the Wiley Online Library or from the author.

Acknowledgements

The research leading to these results has received funding from the European Union Programme for Research and Innovation Horizon 2020 (2014-2020) under the Marie Skłodowska-Curie Grant Agreement PerovSAMs No. 747599, and project INFORM (grant 675867), the Spanish Ministry of Economy and Competitiveness (MINECO) via the Unidad de Excelencia María de Maeztu MDM-2015-0538, MAT2017-88821-R and PCIN-2015-255, and the Generalitat Valenciana (Prometeo/2016/135 and GRISOLIAP/2017/089). H. J. B. acknowledges the support of ERA NET PCIN-2017-014. M. S. thanks the MINECO for his RyC contract. The research leading to these results in the Delft University of Technology has received funding from the European Research Council Horizon 2020 ERC Grant Agreement no. 648433.

Received: ((will be filled in by the editorial staff))

Revised: ((will be filled in by the editorial staff))

Published online: ((will be filled in by the editorial staff))

References

- [1] B. Dänekamp, N. Droseros, F. Palazon, M. Sessolo, N. Banerji, H. J. Bolink, *ACS Appl. Mater. Interfaces* **2018**, acsami.8b13100.
- [2] Q. A. Akkerman, L. Martínez-Sarti, L. Goldoni, M. Imran, D. Baranov, H. J. Bolink, F. Palazon, L. Manna, *Chem. Mater.* **2018**, *30*, 6915.
- [3] D. B. Mitzi, C. A. Feild, Z. Schlesinger, R. B. Laibowitz, *J. Solid State Chem.* **1995**, *114*, 159.
- [4] N. K. Noel, S. D. Stranks, A. Abate, C. Wehrenfennig, S. Guarnera, A. A. Haghighirad, A. Sadhanala, G. E. Eperon, S. K. Pathak, M. B. Johnston, A. Petrozza, L. M. Herz, H. J. Snaith, *Energy Environ. Sci.* **2014**, *7*, 3061.
- [5] Z. Zhao, F. Gu, Y. Li, W. Sun, S. Ye, H. Rao, Z. Liu, **2017**, 1700204.
- [6] J. Jiang, C. K. Onwudinanti, R. A. Hatton, P. A. Bobbert, S. Tao, *J. Phys. Chem. C*

- 2018**, *122*, 17660.
- [7] Z. Chen, J. J. Wang, Y. Ren, C. Yu, K. Shum, Z. Chen, J. J. Wang, Y. Ren, C. Yu, K. Shum, **2012**, *093901*.
- [8] M. H. Kumar, S. Dharani, W. L. Leong, P. P. Boix, R. R. Prabhakar, T. Baikie, C. Shi, H. Ding, R. Ramesh, M. Asta, M. Graetzel, S. G. Mhaisalkar, N. Mathews, *Adv. Mater.* **2014**, *26*, 7122.
- [9] A. Wang, Y. Guo, F. Muhammad, Z. Deng, *Chem. Mater.* **2017**, *29*, 6493.
- [10] N. Wang, Y. Zhou, M. G. Ju, H. F. Garces, T. Ding, S. Pang, X. C. Zeng, N. P. Padture, X. W. Sun, *Adv. Energy Mater.* **2016**, *6*, 1.
- [11] S. Gupta, T. Bendikov, G. Hodes, D. Cahen, *ACS Energy Lett.* **2016**, *1*, 1028.
- [12] A. G. Kontos, A. Kaltzoglou, E. Siranidi, D. Palles, G. K. Angeli, M. K. Arfanis, V. Psycharis, Y. S. Raptis, E. I. Kamitsos, P. N. Trikalitis, C. C. Stoumpos, M. G. Kanatzidis, P. Falaras, *Inorg. Chem.* **2017**, *56*, 84.
- [13] P. Xu, S. Chen, H. J. Xiang, X. G. Gong, S. H. Wei, *Chem. Mater.* **2014**, *26*, 6068.
- [14] I. Chung, J. H. Song, J. Im, J. Androulakis, C. D. Malliakas, H. Li, A. J. Freeman, J. T. Kenney, M. G. Kanatzidis, *J. Am. Chem. Soc.* **2012**, *134*, 8579.
- [15] F. Hao, C. C. Stoumpos, D. H. Cao, R. P. H. Chang, M. G. Kanatzidis, *Nat. Photonics* **2014**.
- [16] L. Y. Huang, W. R. L. Lambrecht, *Phys. Rev. B - Condens. Matter Mater. Phys.* **2013**, *88*, 1.
- [17] W. Li, J. Li, J. Li, J. Fan, Y. Mai, L. Wang, *J. Mater. Chem. A* **2016**, *4*, 17104.
- [18] D. Sabba, H. K. Mulmudi, R. R. Prabhakar, T. Krishnamoorthy, T. Baikie, P. P. Boix, S. Mhaisalkar, N. Mathews, *J. Phys. Chem. C* **2015**, *119*, 1763.
- [19] C. Grote, R. F. Berger, *J. Phys. Chem. C* **2015**, *119*, 22832.
- [20] G. Fisher, **1973**, *14*, 308.
- [21] C. G. Ma, V. Krasnenko, M. G. Brik, *J. Phys. Chem. Solids* **2018**, *115*, 289.

- [22] E. L. Da Silva, J. M. Skelton, S. C. Parker, A. Walsh, *Phys. Rev. B - Condens. Matter Mater. Phys.* **2015**, *91*, 1.
- [23] K. P. Marshall, M. Walker, R. I. Walton, R. A. Hatton, *J. Mater. Chem. A* **2017**, *5*, 21836.
- [24] K. P. Marshall, M. Walker, R. I. Walton, R. A. Hatton, *Nat. Energy* **2016**, *1*, 1.
- [25] Y. K. Jung, J. H. Lee, A. Walsh, A. Soon, *Chem. Mater.* **2017**, *29*, 3181.
- [26] F. Hao, C. C. Stoumpos, R. P. H. Chang, M. G. Kanatzidis, **2014**.
- [27] G. Thiele, B. R. Serr, *Zeitschrift fur Krist. - New Cryst. Struct.* **1995**, *210*, 64.
- [28] K. P. Marshall, S. Tao, M. Walker, D. S. Cook, J. Lloyd-Hughes, S. Varagnolo, A. Wijesekara, D. Walker, R. I. Walton, R. A. Hatton, *Mater. Chem. Front.* **2018**, *2*, 1515.
- [29] F. Wang, J. Ma, F. Xie, L. Li, J. Chen, J. Fan, N. Zhao, **2016**, 3417.
- [30] T. Song, T. Yokoyama, C. C. Stoumpos, J. Logsdon, D. H. Cao, M. R. Wasielewski, S. Aramaki, M. G. Kanatzidis, **2017**.
- [31] F. Chiarella, A. Zappettini, F. Licci, I. Borriello, G. Cantele, D. Ninno, A. Cassinese, R. Vaglio, *Phys. Rev. B - Condens. Matter Mater. Phys.* **2008**, *77*, 1.
- [32] W. Liao, D. Zhao, Y. Yu, C. R. Grice, C. Wang, A. J. Cimaroli, P. Schulz, W. Meng, K. Zhu, R. Xiong, Y. Yan, **2016**, 9333.
- [33] S. J. Lee, S. S. Shin, Y. C. Kim, D. Kim, T. K. Ahn, J. H. Noh, J. Seo, S. Il Seok, *J. Am. Chem. Soc.* **2016**, *138*, 3974.
- [34] S. Shao, J. Liu, G. Portale, H. H. Fang, G. R. Blake, G. H. ten Brink, L. J. A. Koster, M. A. Loi, *Adv. Energy Mater.* **2018**, *8*.
- [35] D. Zhao, C. Chen, C. Wang, M. M. Junda, Z. Song, C. R. Grice, Y. Yu, C. Li, B. Subedi, N. J. Podraza, X. Zhao, G. Fang, R. Xiong, K. Zhu, Y. Yan, *Nat. Energy* **2018**, *3*, 1093.
- [36] I. Chung, B. Lee, J. He, R. P. H. Chang, M. G. Kanatzidis, *Nature* **2012**, *485*, 486.
- [37] B. Lee, C. C. Stoumpos, N. Zhou, F. Hao, C. Malliakas, C. Y. Yeh, T. J. Marks, M. G.

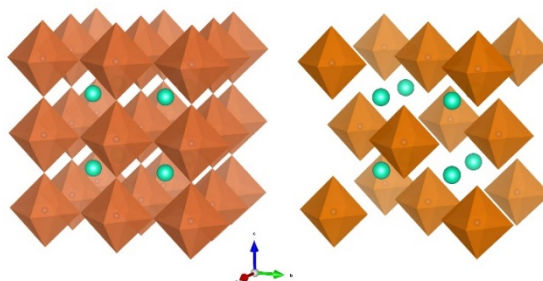
- Kanatzidis, R. P. H. Chang, *J. Am. Chem. Soc.* **2014**, *136*, 15379.
- [38] Z. Xiao, H. Lei, X. Zhang, Y. Zhou, H. Hosono, T. Kamiya, *Bull. Chem. Soc. Jpn.* **2015**, *88*, 1250.
- [39] A. Kaltzoglou, M. Antoniadou, A. G. Kontos, C. C. Stoumpos, D. Perganti, E. Siranidi, V. Raptis, K. Trohidou, V. Psycharis, M. G. Kanatzidis, P. Falaras, *J. Phys. Chem. C* **2016**, *120*, 11777.
- [40] A. Kaltzoglou, M. Antoniadou, D. Perganti, E. Siranidi, V. Raptis, K. Trohidou, V. Psycharis, A. G. Kontos, P. Falaras, *Electrochim. Acta* **2015**, *184*, 466.
- [41] B. Saparov, J. P. Sun, W. Meng, Z. Xiao, H. S. Duan, O. Gunawan, D. Shin, I. G. Hill, Y. Yan, D. B. Mitzi, *Chem. Mater.* **2016**, *28*, 2315.
- [42] Z. Tan, J. Li, C. Zhang, Z. Li, Q. Hu, Z. Xiao, T. Kamiya, H. Hosono, G. Niu, E. Lifshitz, Y. Cheng, J. Tang, *Adv. Funct. Mater.* **2018**, *1801131*, doi: 10.1002/adfm.201801131.
- [43] A. E. Maughan, A. M. Ganose, A. M. Candia, J. T. Granger, D. O. Scanlon, J. R. Neilson, *Chem. Mater.* **2018**, *30*, 472.
- [44] A. E. Maughan, A. M. Ganose, M. A. Almaker, D. O. Scanlon, J. R. Neilson, *Chem. Mater.* **2018**, *30*, 3909.
- [45] Z. Xiao, Y. Zhou, H. Hosono, T. Kamiya, *Phys. Chem. Chem. Phys.* **2015**, *17*, 18900.
- [46] X. Qiu, B. Cao, S. Yuan, X. Chen, Z. Qiu, Y. Jiang, Q. Ye, H. Wang, H. Zeng, J. Liu, M. G. Kanatzidis, *Sol. Energy Mater. Sol. Cells* **2017**, *159*, 227.
- [47] J. C. R. Ke, D. J. Lewis, A. S. Walton, B. F. Spencer, P. O'Brien, A. G. Thomas, W. R. Flavell, *J. Mater. Chem. A* **2018**, *6*, 11205.
- [48] B. Lee, A. Krenselewski, S. Il Baik, D. N. Seidman, R. P. H. Chang, *Sustain. Energy Fuels* **2017**, *1*, 710.
- [49] O. Y. Posudievsky, N. V. Konoshchuk, V. L. Karbivskyy, O. P. Boiko, V. G. Koshechko, V. D. Pokhodenko, *Theor. Exp. Chem.* **2017**, *53*, 235.

- [50] D. Prochowicz, P. Yadav, M. Saliba, D. J. Kubicki, M. M. Tavakoli, S. M. Zakeeruddin, J. Lewiński, L. Emsley, M. Grätzel, *Nano Energy* **2018**, *49*, 523.
- [51] A. Karmakar, A. M. Askar, G. M. Bernard, V. V. Terskikh, M. Ha, S. Patel, K. Shankar, V. K. Michaelis, *Chem. Mater.* **2018**, *30*, 2309.
- [52] Y. El Ajjouri, F. Palazon, M. Sessolo, H. J. Bolink, *Chem. Mater.* **2018**, *30*, 7423.
- [53] D. J. Kubicki, D. Prochowicz, A. Hofstetter, S. M. Zakeeruddin, M. Grätzel, L. Emsley, *J. Am. Chem. Soc.* **2018**, *140*, 7232.
- [54] Z. Y. Zhu, Q. Q. Yang, L. F. Gao, L. Zhang, A. Y. Shi, C. L. Sun, Q. Wang, H. L. Zhang, *J. Phys. Chem. Lett.* **2017**, *8*, 1610.
- [55] D. Prochowicz, M. Franckevičius, A. M. Cieślak, S. M. Zakeeruddin, M. Grätzel, J. Lewiński, *J. Mater. Chem. A* **2015**, *3*, 20772.
- [56] A. D. Jodlowski, A. Yépez, R. Luque, L. Camacho, G. de Miguel, *Angew. Chemie - Int. Ed.* **2016**, *55*, 14972.
- [57] L. Protesescu, S. Yakunin, O. Nazarenko, D. N. Dirin, M. V. Kovalenko, *ACS Appl. Nano Mater.* **2018**, *1*, 1300.
- [58] D. J. Kubicki, D. Prochowicz, A. Hofstetter, S. M. Zakeeruddin, M. Grätzel, L. Emsley, *J. Am. Chem. Soc.* **2017**, *139*, 14173.
- [59] M. Saski, D. Prochowicz, W. Marynowski, J. Lewinski, *Eur. J. Inorg. Chem.* **2019**, *3*.
- [60] Y. E. El Ajjouri, V. S. S. S. Chirvony, M. Sessolo, Y. El Ajjouri, V. S. Chirvony, M. Sessolo, F. Palazon, H. J. Bolink, *RSC Adv.* **2018**, *8*, 41548.
- [61] J. V. Milić, J. H. Im, D. J. Kubicki, A. Ummadisingu, J. Y. Seo, Y. Li, M. A. Ruiz-Preciado, M. I. Dar, S. M. Zakeeruddin, L. Emsley, M. Grätzel, *Adv. Energy Mater.* **2019**, *1900284*, 1.
- [62] A. Karmakar, M. S. Dodd, X. Zhang, M. S. Oakley, M. Klobukowski, V. K. Michaelis, *Chem. Commun.* **2019**, *55*, 5079.
- [63] Y. El Ajjouri, V. S. Chirvony, N. Vassilyeva, M. Sessolo, F. Palazon, H. J. Bolink, *J.*

Mater. Chem. C **2019**.

- [64] J. Breternitz, S. Levchenko, H. Hempel, G. Gurieva, A. Franz, A. Hoser, S. Schorr, *J. Phys. Energy* **2018**, *1*, 25003.
- [65] O. Y. Posudievsky, N. V. Konoshchuk, A. G. Shkavro, V. L. Karbivskiy, V. G. Koshechko, V. D. Pokhodenko, *ACS Appl. Nano Mater.* **2018**, *1*, 4145.
- [66] S. Yun, A. Kirakosyan, S. G. Yoon, J. Choi, *ACS Sustain. Chem. Eng.* **2018**, *6*, 3733.
- [67] M. Wilke, N. Casati, *Chem. - A Eur. J.* **2018**.
- [68] D. Prochowicz, P. Yadav, M. Saliba, M. Saski, S. M. Zakeeruddin, J. Lewiński, M. Grätzel, *Sustain. Energy Fuels* **2017**, *1*.
- [69] P. Pal, S. Saha, A. Banik, A. Sarkar, K. Biswas, *Chem. - A Eur. J.* **2018**, *24*, 1811.
- [70] A. M. Askar, A. Karmakar, G. M. Bernard, M. Ha, V. V. Terskikh, B. D. Wiltshire, S. Patel, J. Fleet, K. Shankar, V. K. Michaelis, *J. Phys. Chem. Lett.* **2018**, *9*, 2671.
- [71] C. C. Stoumpos, C. D. Malliakas, M. G. Kanatzidis, *Inorg. Chem.* **2013**, *52*, 9019.
- [72] T. Leijtens, R. Prasanna, A. Gold-Parker, M. F. Toney, M. D. McGehee, *ACS Energy Lett.* **2017**, *2*, 2159.
- [73] Y. Dang, Y. Zhou, X. Liu, D. Ju, S. Xia, H. Xia, X. Tao, *Angew. Chemie - Int. Ed.* **2016**, *55*, 3447.
- [74] I. Lignos, L. Protesescu, D. B. Emiroglu, R. MacEiczyk, S. Schneider, M. V. Kovalenko, A. J. DeMello, *Nano Lett.* **2018**, *18*, 1246.
- [75] K. Wang, Z. Jin, L. Liang, H. Bian, D. Bai, H. Wang, J. Zhang, Q. Wang, L. Shengzhong, *Nat. Commun.* **2018**, *9*, 1.
- [76] L. Jie, X. Chao, *J. Non. Cryst. Solids* **1990**, *119*, 37.
- [77] G. Sadoughi, D. E. Starr, E. Handick, S. D. Stranks, M. Gorgoi, R. G. Wilks, M. Bär, H. J. Snaith, *ACS Appl. Mater. Interfaces* **2015**, *7*, 13440.
- [78] H. Cho, S. H. Jeong, M. H. Park, Y. H. Kim, C. Wolf, C. L. Lee, J. H. Heo, A. Sadhanala, N. S. Myoung, S. Yoo, S. H. Im, R. H. Friend, T. W. Lee, *Science (80-)*.

- 2015**, 350, 1222.
- [79] W. Zhang, S. Pathak, N. Sakai, T. Stergiopoulos, P. K. Nayak, N. K. Noel, A. A. Haghghirad, V. M. Burlakov, D. W. Dequillettes, A. Sadhanala, W. Li, L. Wang, D. S. Ginger, R. H. Friend, H. J. Snaith, *Nat. Commun.* **2015**, 6, 1.
- [80] A. Calloni, A. Abate, G. Bussetti, G. Berti, R. Yivlialin, F. Ciccacci, L. Duò, *J. Phys. Chem. C* **2015**, 119, 21329.
- [81] G. Abdelmageed, L. Jewell, K. Hellier, L. Seymour, B. Luo, F. Bridges, J. Z. Zhang, S. Carter, *Appl. Phys. Lett.* **2016**, 109, 0.
- [82] D. Meggiolaro, S. G. Motti, E. Mosconi, A. J. Barker, J. Ball, C. Andrea Riccardo Perini, F. Deschler, A. Petrozza, F. De Angelis, *Energy Environ. Sci.* **2018**, 11, 702.
- [83] W. Ke, C. C. Stoumpos, M. G. Kanatzidis, *Adv. Mater.* **2018**, 1803230.
- [84] D. Zhao, Y. Yu, C. Wang, W. Liao, N. Shrestha, C. R. Grice, A. J. Cimaroli, L. Guan, R. J. Ellingson, K. Zhu, X. Zhao, R. G. Xiong, Y. Yan, *Nat. Energy* **2017**, 2, 1.
- [85] S. J. Lee, S. S. Shin, J. Im, T. K. Ahn, J. H. Noh, N. J. Jeon, S. Il Seok, J. Seo, *ACS Energy Lett.* **2018**, 3, 46.
- [86] H. O. Shin, B. M. Kim, T. Jang, K. M. Kim, D. H. Roh, J. S. Nam, J. S. Kim, U. Y. Kim, B. Lee, Y. Pang, T. H. Kwon, *Adv. Energy Mater.* **2019**, 9, 1.
- [87] J. Warman, M. De Haas, G. Dicker, F. Grozema, *Chem. Mater* **2004**, 4600.
- [88] T. Leijtens, R. Prasanna, K. A. Bush, G. E. Eperon, J. A. Raiford, A. Gold-Parker, E. J. Wolf, S. A. Swifter, C. C. Boyd, H. P. Wang, M. F. Toney, S. F. Bent, M. D. McGehee, *Sustain. Energy Fuels* **2018**, 2, 2450.
- [89] M. C. Gélvez-Rueda, D. H. Cao, S. Patwardhan, N. Renaud, C. C. Stoumpos, G. C. Schatz, J. T. Hupp, O. K. Farha, T. J. Savenije, M. G. Kanatzidis, F. C. Grozema, *J. Phys. Chem. C* **2016**, 120, 16577.
- [90] M. C. Gélvez-Rueda, N. Renaud, F. C. Grozema, *J. Phys. Chem. C* **2017**, 121, 23392.



Scheme 1. Crystal structures of CsSnI_3 (left) and Cs_2SnI_6 (right). Green balls represent Cs^+ ions and orange octahedra represent SnI_6 units. Cs_2SnI_6 crystal structure can be viewed as a derivative from CsSnI_3 where every other SnI_6 octahedra is removed (the oxidation state of Sn is consequently +2 in CsSnI_3 and +4 in Cs_2SnI_6).

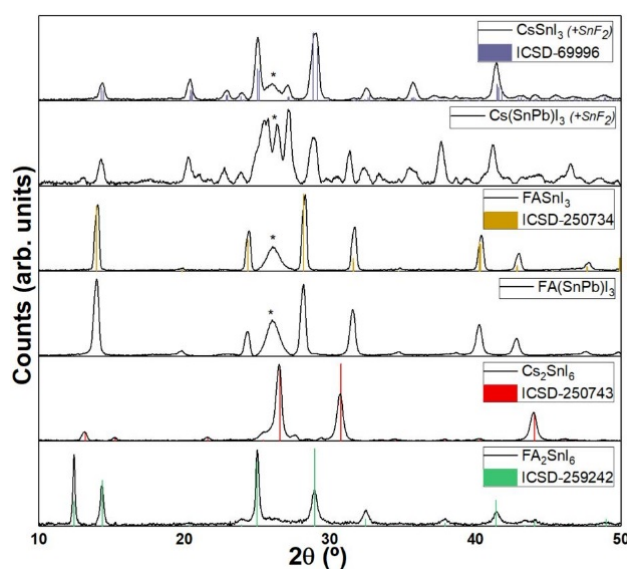


Figure 1. XRD diffractograms of mechanochemically synthesized tin perovskites (black lines) together with reference bulk patterns from Inorganic Crystal Structure Database (ICSD; color columns). A broad peak around $2\theta = 26^\circ$ and marked with an asterisk is visible in most diffractograms due to parasitic diffraction from the adhesive tape used to fix the powder samples

on the substrate (see Figure S1). No reference pattern is available for mixed tin-lead perovskites. However, main peaks' positions match the reference pure-tin counterpart with a slight shift to lower angles due to the incorporation of the larger lead cation (see Figure S2).

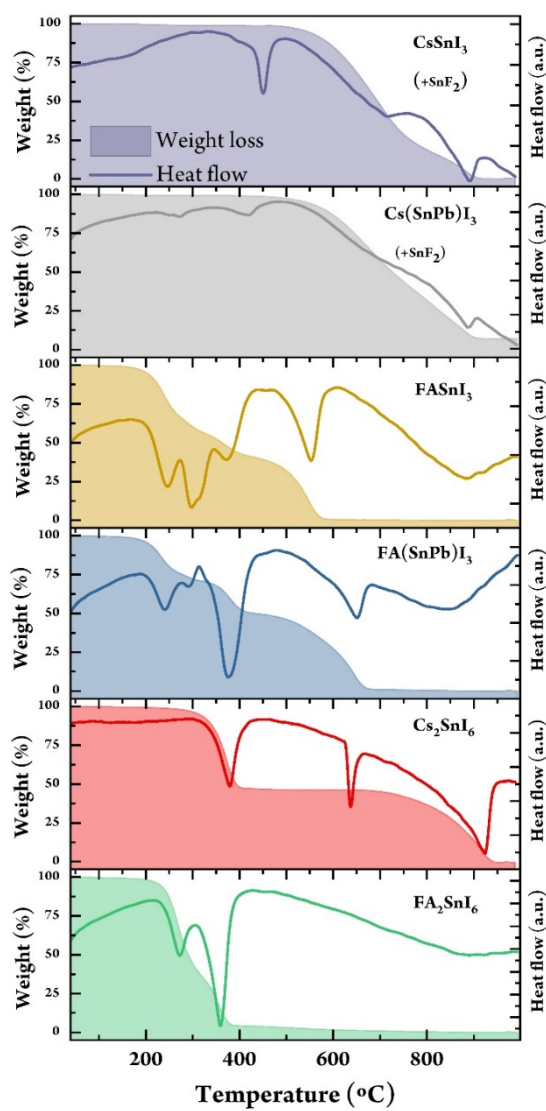


Figure 2. TG (filled area) and DTA (simple line) curves of all compounds in the 40 °C to 1000 °C range.

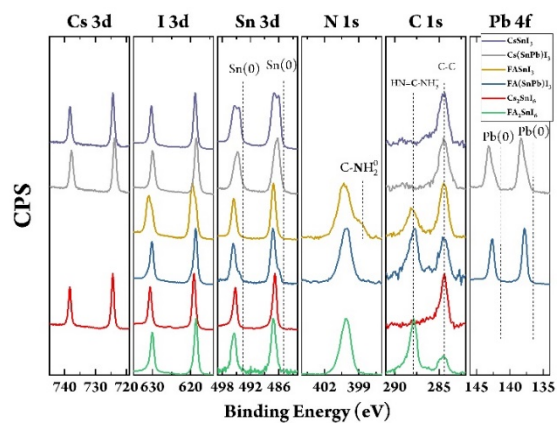


Figure 3. High-resolution XPS spectra of all main elements from the different compounds: Cs 3d, I 3d, Sn 3d, N 1s, C 1s, and Pb 4f regions. Additional O 1s and F 1s spectra are given as supporting information in Figures S6 and S7.

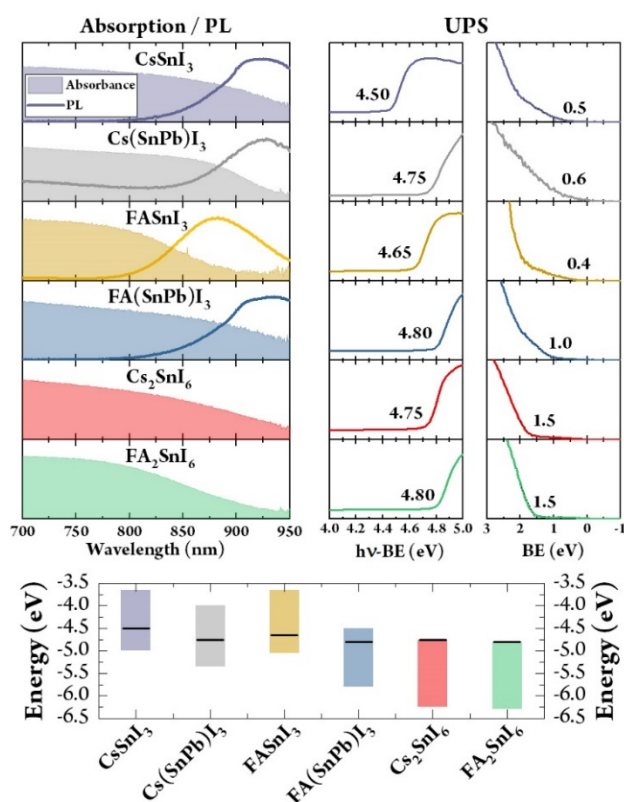


Figure 4. Optical characterization, UPS, and derived energy diagram.

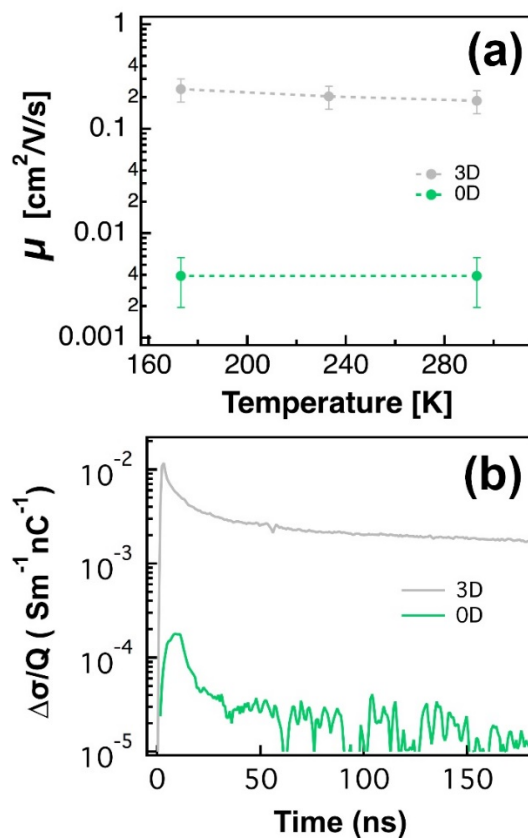


Figure 5. Mobility of charge carriers as a function of temperature (a) and change of conductivity as a function of time (b) of a Sn(II) 3D perovskite (grey) and a Sn(IV) 0D vacancy-ordered perovskite (green).

Table 1. Atomic percentages of relevant elements based on high-resolution XPS spectra.

	Cs	I	Sn	N	C	Pb
	at. %					
CsSnI₃	23.8	50.6	25.5	-	-	-
Cs(SnPb)I₃	26.4	50.7	11.5	-	-	11.4
FASnI₃	-	25.9	21.2	34.6	17.7	-
FA(SnPb)I₃	-	34.5	9.3	31.0	17.0	8.2

Cs₂SnI₆	28.0	57.3	14.7	-	-	-
FA₂SnI₆	-	26.8	1.2	47.4	24.6	-

Supporting Information

Mechanochemical Synthesis of Sn(II) and Sn(IV) Iodide Perovskites and Study of Their Structural, Chemical, Thermal, Optical and Electrical Properties

Yousra El Ajjouri, Federico Locardi, María C. Gélvez-Rueda, Mirko Prato, Michele Sessolo, Maurizio Ferretti, Ferdinand C. Grozema, Francisco Palazon* and Henk J. Bolink

Experimental details:

Materials. Cesium iodide (CsI, > 99 %), tin(II) iodide (SnI₂, > 97 %) and lead iodide (PbI₂, 99.99 %) were purchased from TCI. Tin fluoride (SnF₂, 99%) and tin(IV) iodide (SnI₄, 99.999 %) were purchased from Sigma-Aldrich. Formamidinium iodide (CH₅N₂I) was purchased from GreatCell Solar. All chemicals were stored in a nitrogen-filled glovebox and used as received without further purification.

Mechanochemical Synthesis. AI:SnI₂ (1:1), AI:(Sn_{0.5}Pb_{0.5})I₂ (1:1) and AI:SnI₄ (2:1) powders (A = Cs or FA) were mixed inside a nitrogen-filled glovebox. Then, approximately 3 grams of the mixed precursors powder was introduced inside 10 mL zirconia ball-mill jars with 2 zirconia beads of 10 mm in diameter. The jars were closed under nitrogen, preventing the powders to be exposed to air. Eventually ball milling was performed with a MM-400 straight ball-mill from Retsch, at a frequency of 30 Hz for 5 hours.

XRD. X-ray diffraction was measured with a Panalytical Empyrean diffractometer equipped with CuK α anode operated at 45 kV and 30 mA and a Pixel 1D detector in scanning line mode. Single scans were acquired in the $2\Theta = 10^\circ$ to 50° range in Bragg-Brentano geometry in air. Data analysis was performed with HighScore Plus software.

DTA/TG. Differential thermal analysis (DTA)/thermogravimetry (TG) were performed using a LabsysEvo 1600 DTA/TGA (Setaram). The samples (~ 15 mg) were put in an alumina crucible and heated from 30 to 1000 °C, at 45 °C min⁻¹ under an He atmosphere (30 ml min⁻¹). The DTA and TGA curves were elaborated using the dedicated software Calisto (Setaram).

X-ray and ultraviolet photoelectron spectroscopy. The measurements were carried out with a Kratos Axis UltraDLDSpectrometer. For XPS measurements, high-resolution spectra were acquired at a pass energy of 10 eV using a monochromatic Al K α source (15 kV, 20 mA). The UPS measurements were performed using a He I (21.22 eV) discharge lamp, on an area of 55 μ m in diameter, at a pass energy of 5 eV and with a dwell time of 100ms. The work function (that is, the position of the Fermi level with respect to the vacuum level) was measured from the threshold energy for the emission of secondary electrons during He I excitation. A -9.0 V bias was applied to the sample to precisely determine the low-kinetic-energy cutoff. Then, the position of the VBM versus the vacuum level was estimated by measuring its distance from the Fermi level.

Optical characterization. Absorbance was measured with a High Power UV-VIS fiber light source, integrated sphere and Avantes Starline AVASpec-2048L spectrometer in reflection mode. Photoluminescence was measured with a continuous wave 375 nm diode laser with a 400nm filter, and Hamamatsu PMA 11 spectrometer. For a typical spectrum 10 scans of 1 second were averaged.

Pulse-radiolysis microwave conductivity measurements. Microwave conductivity measurements with irradiation by a high-energy electron pulse were made on micrometer crystals (~45 mg) placed in a Polyether ether ketone (PEEK) holder. The PEEK holder is placed inside a rectangular waveguide cell (made of chemically inert gold-plated copper). The cell is contained in a cryostat in which the temperature can be varied between 123K and 473K. The

irradiation intensity was varied between pulse lengths of 0.2 ns to 10 ns (charge carrier concentrations $\sim 1 \times 10^{15} \text{ cm}^{-3}$ to $8 \times 10^{16} \text{ cm}^{-3}$). The frequency scan (28-38 GHz) fits were measured at a pulse length of 0.5 ns ($\sim 5.8 \times 10^{15} \text{ cm}^{-3}$).

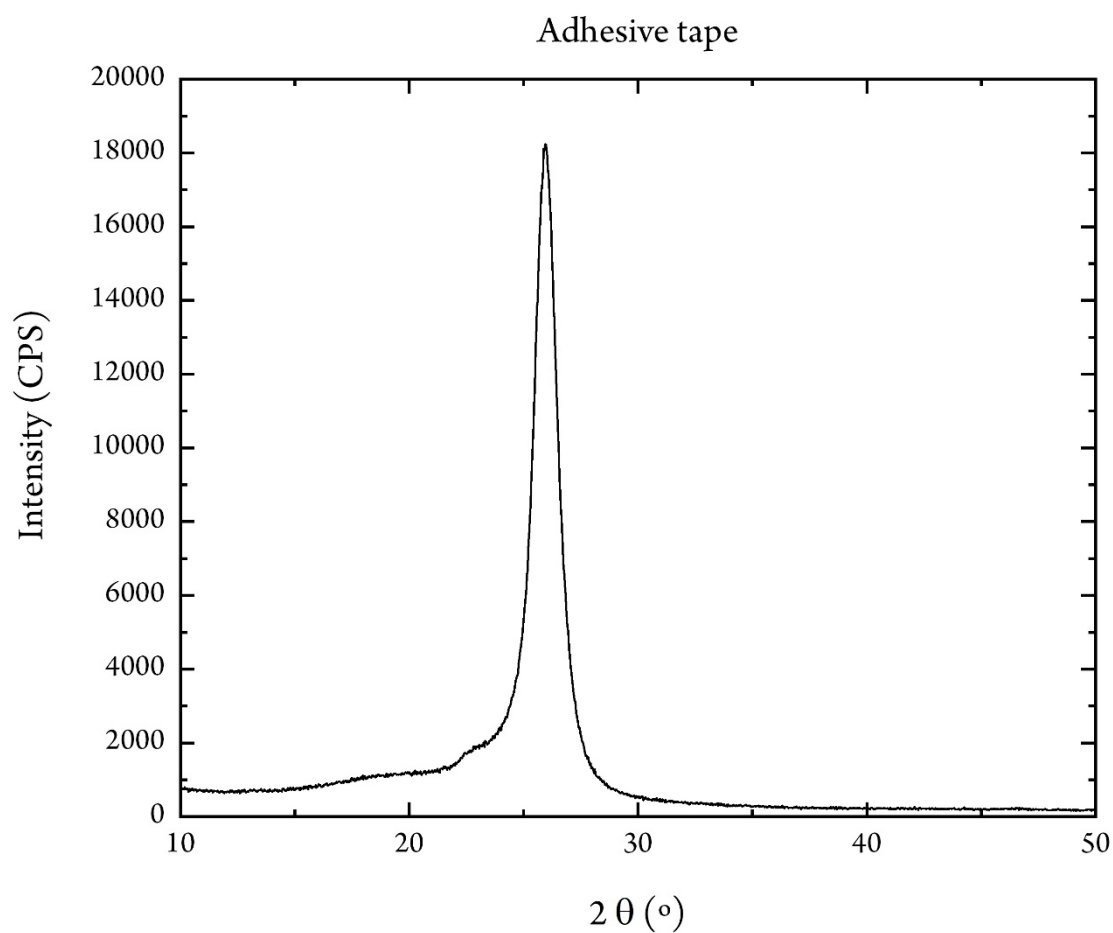


Figure S 1. X-ray diffractogram of adhesive tape used to fix powders on glass substrates.

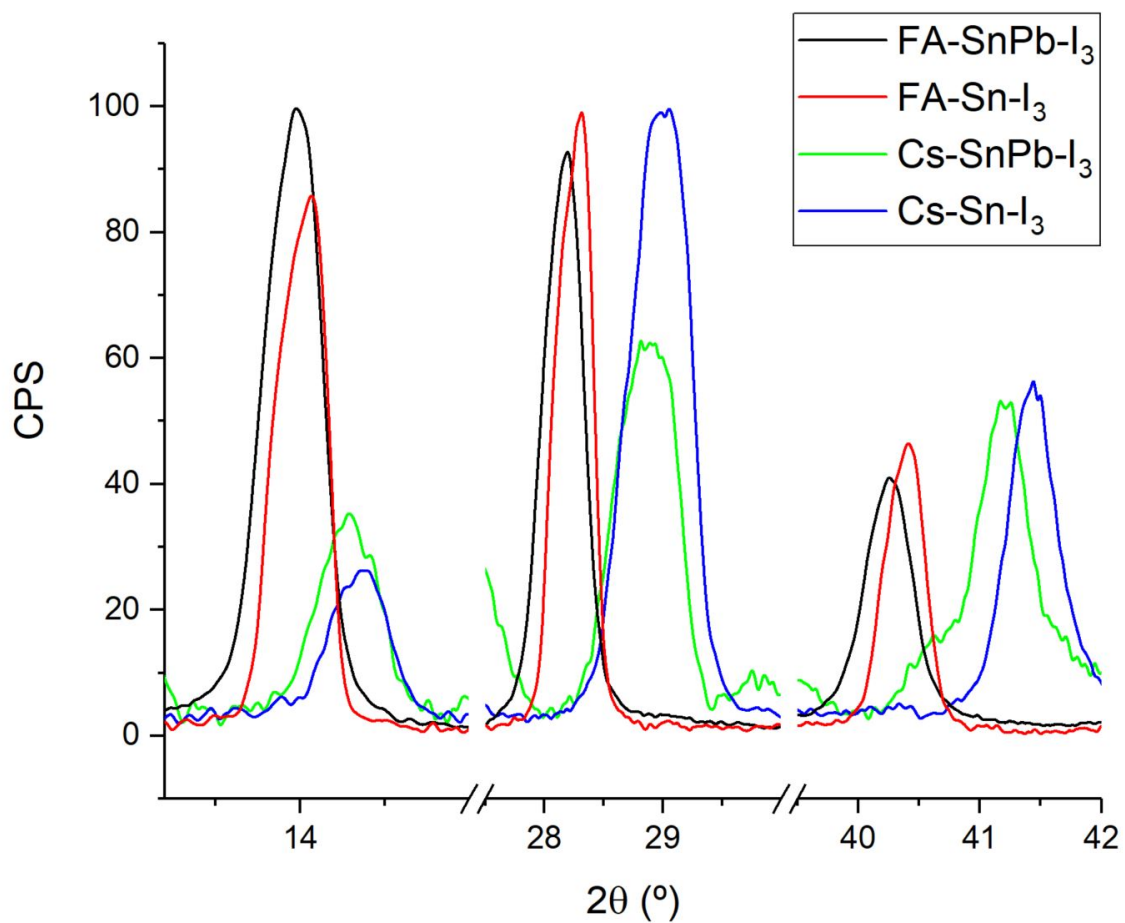


Figure S 2. Most representative parts of X-ray diffractograms presented in Figure 1 for CsSnI₃, Cs(SnPb)I₃, FASnI₃, and FA(SnPb)I₃. Larger ions induce a shift towards lower diffraction angles.

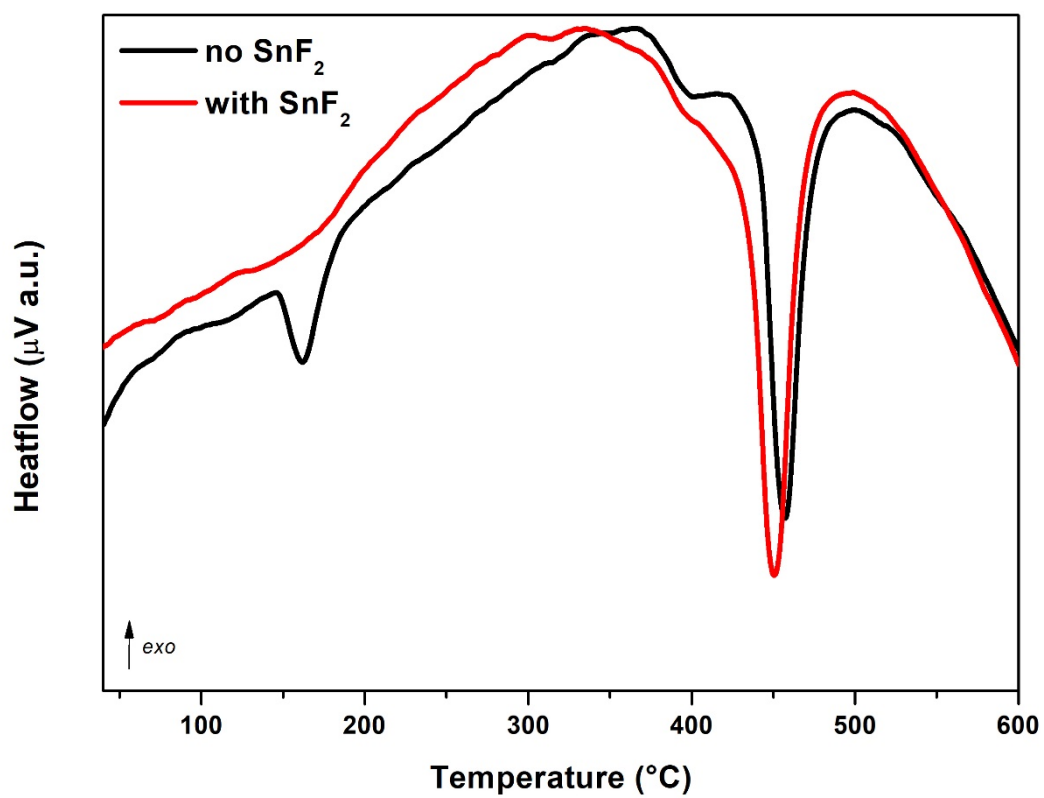


Figure S 3. Differential thermal analysis of ball-milled $\text{CsI}+\text{SnI}_2$ with (red curve) and without SnF_2 (black curve). SnI_4 is detected (identified by the peak at $\sim 160^{\circ}\text{C}$ in the black curve) only in absence of SnF_2 .

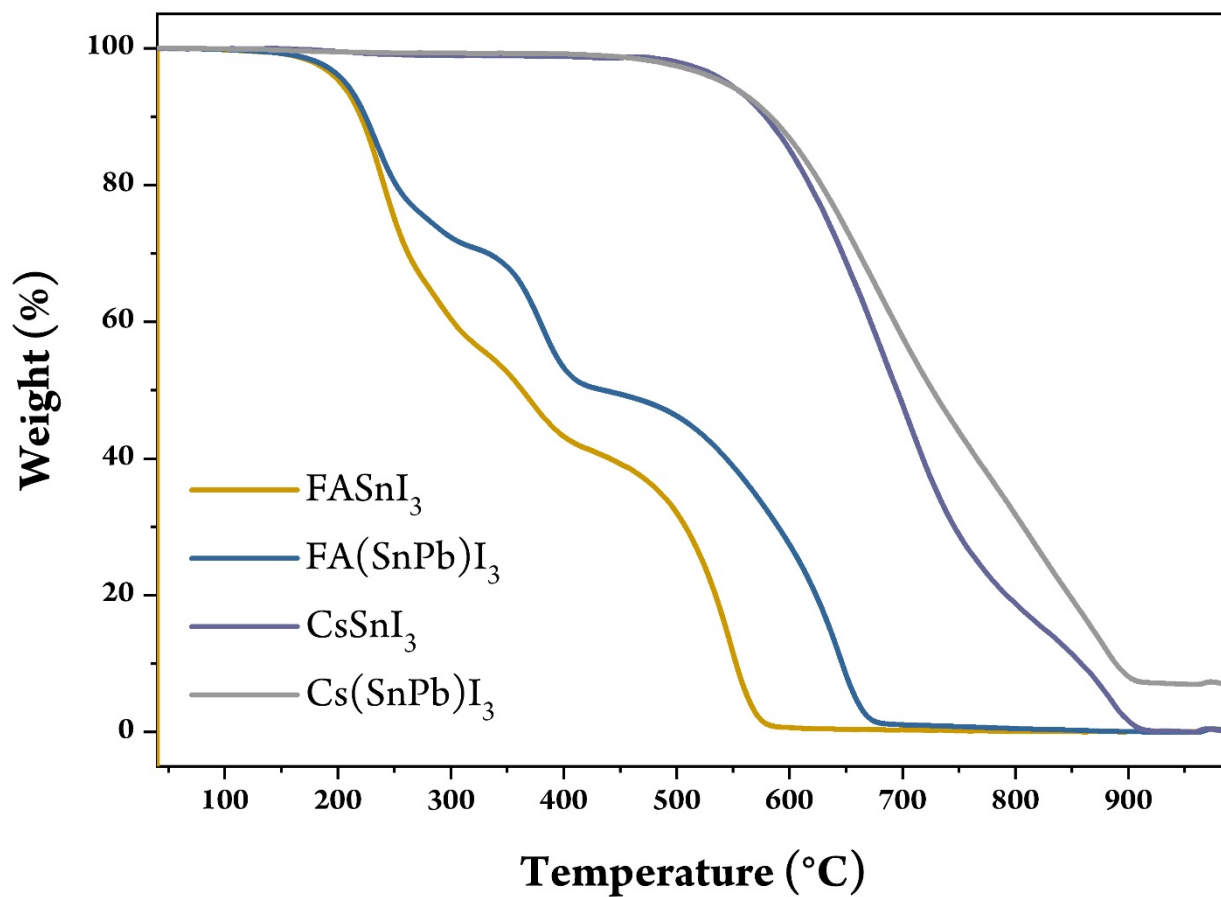


Figure S4. Comparison between thermogravimetric curves of $A\text{SnI}_3$ and $A(\text{SnPb})\text{I}_3$ ($A = \text{Cs}$ or FA).

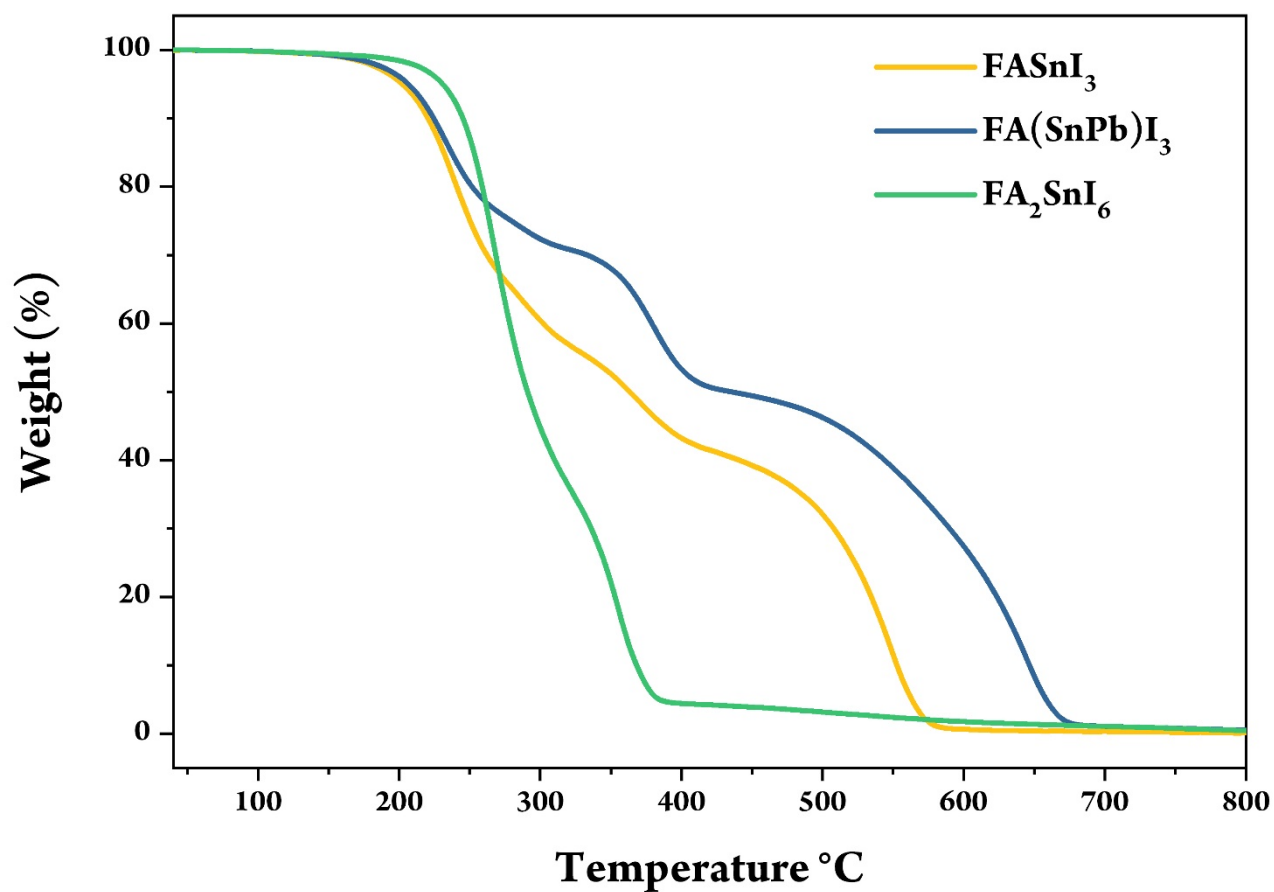


Figure S5. Comparison between thermogravimetric curves of FASnI_3 , FA(SnPb)I_3 and $\text{FA}_2\text{SnPbI}_6$

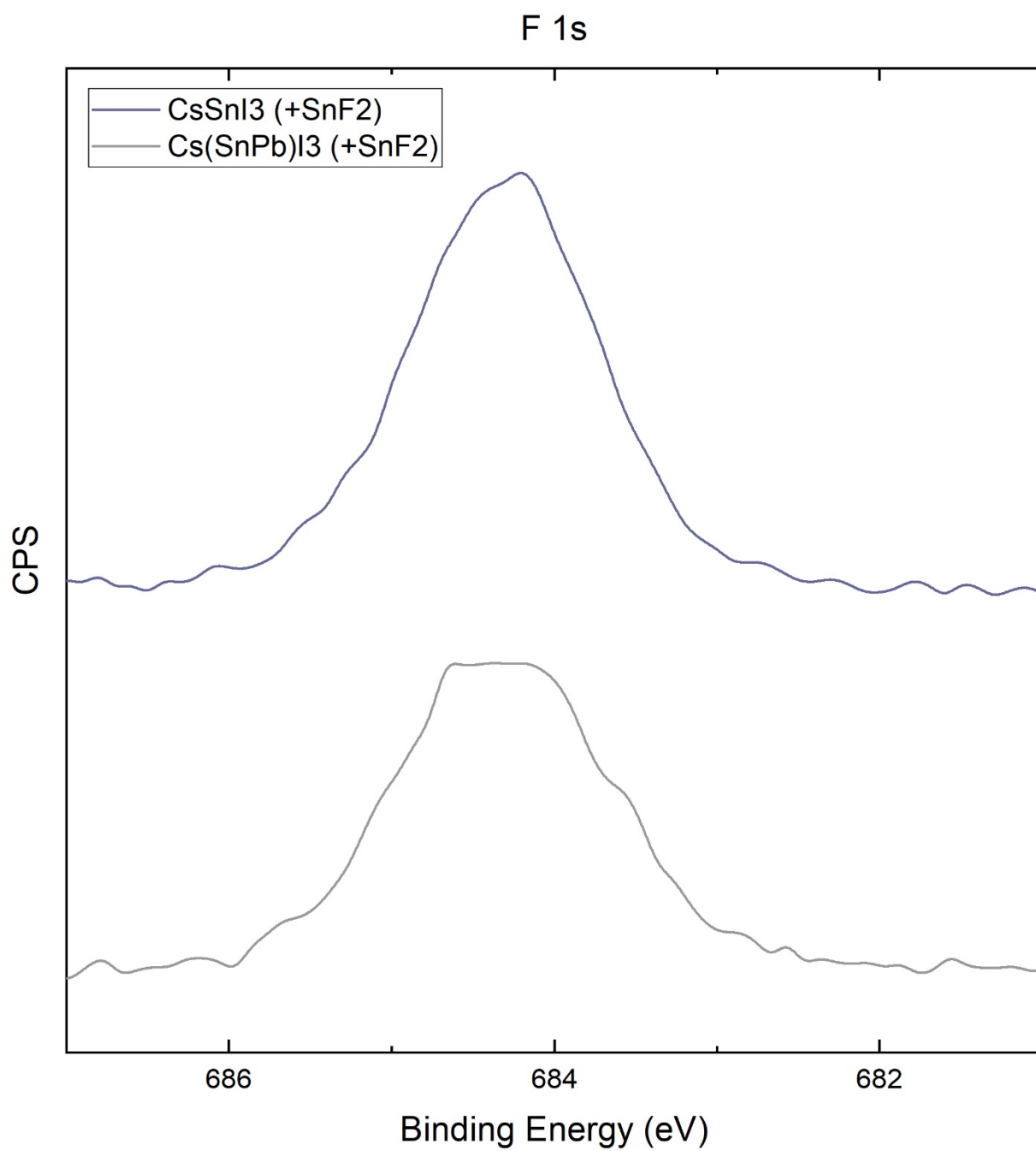


Figure S 6. F1s XPS spectra of CsSnI₃ and Cs(SnPb)I₃ prepared with addition of SnF₂.

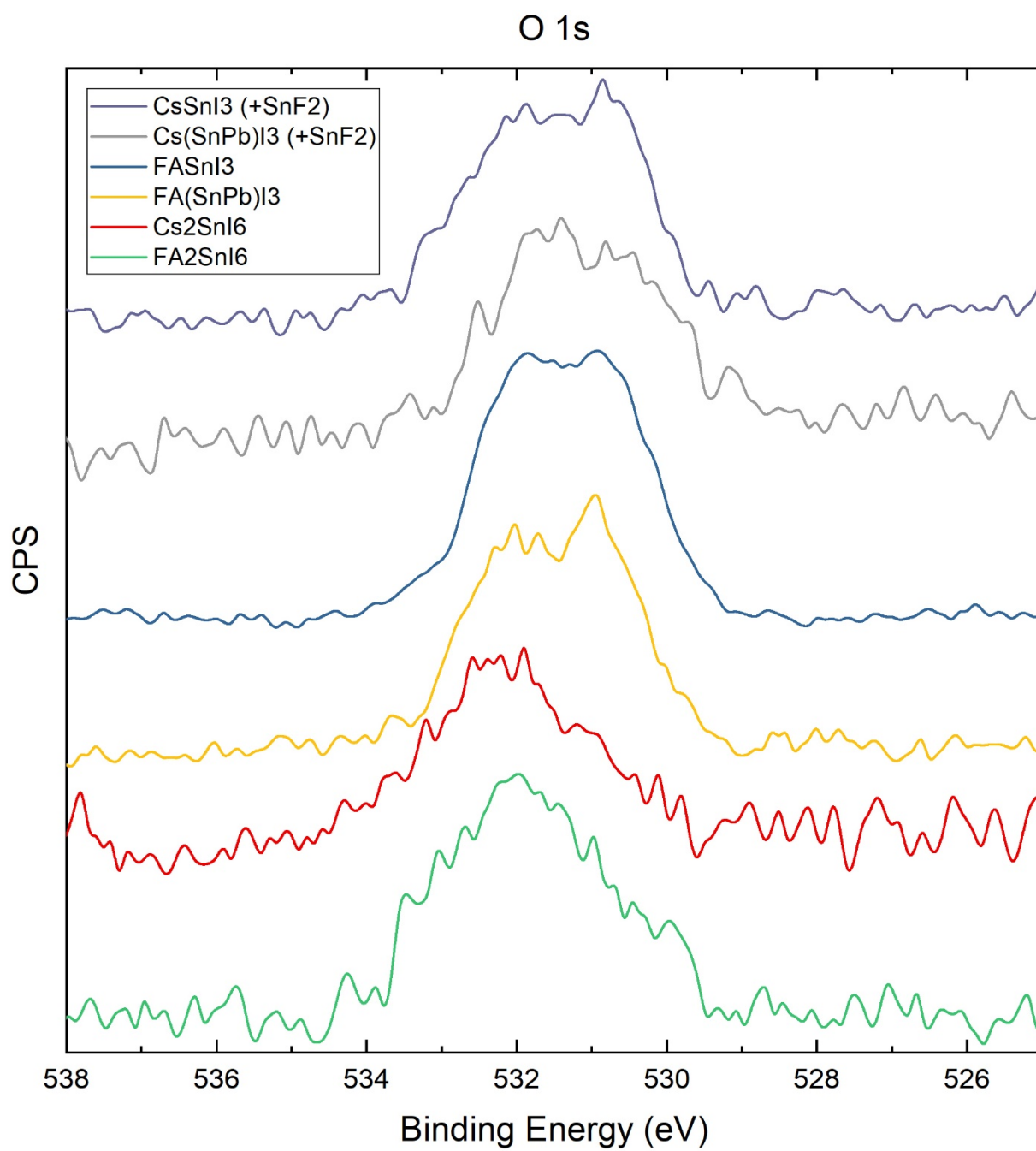


Figure S 7. O 1s XPS spectra of all compounds.

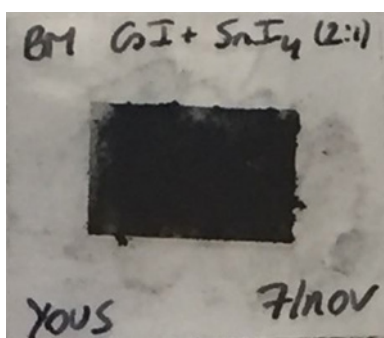


Figure S 8. Photograph of Cs₂SnI₆ powder fixed on adhesive tape on a glass substrate. The sample is in air.

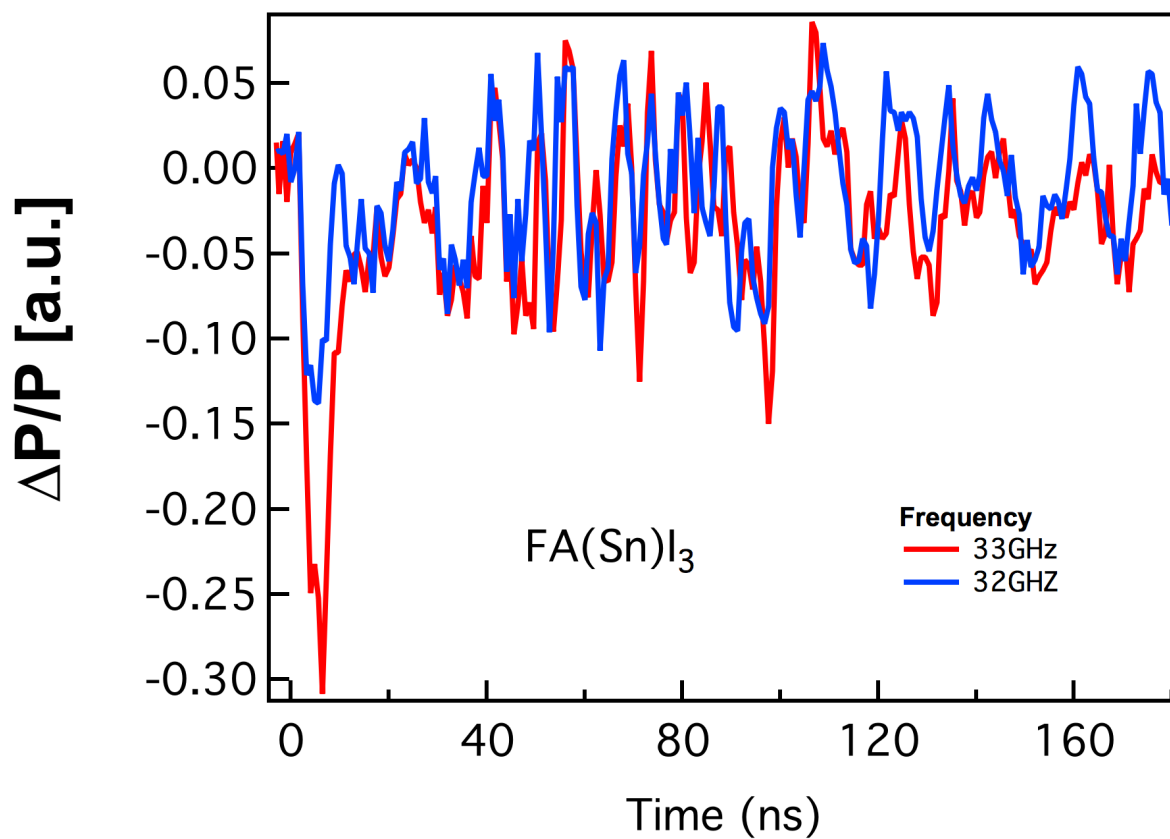


Figure S 9. Change of reflected microwave power as a function of time for FASnI₃. Shown at different microwave frequencies (32 to 33 GHz).

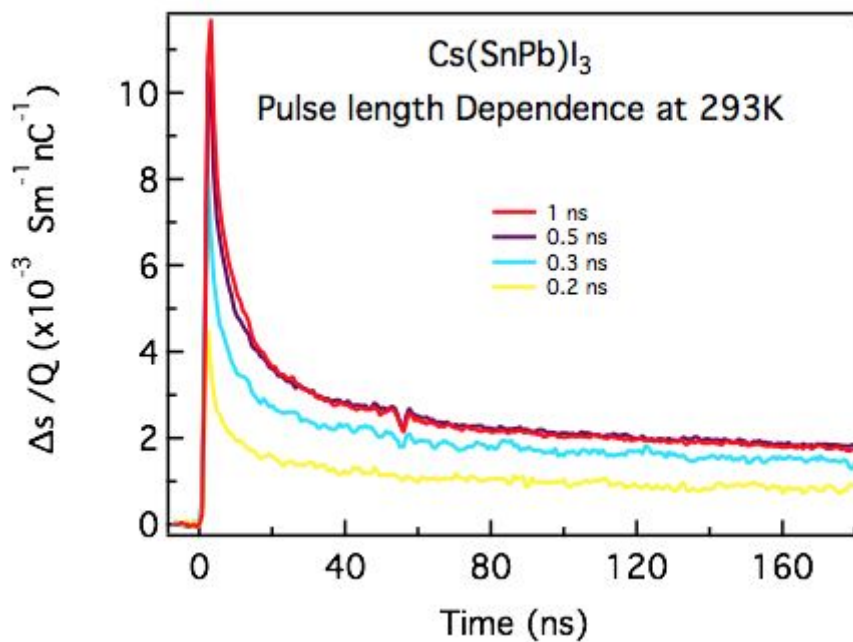


Figure S 10. Charge carrier lifetime of the 3D sample at different pulse widths.

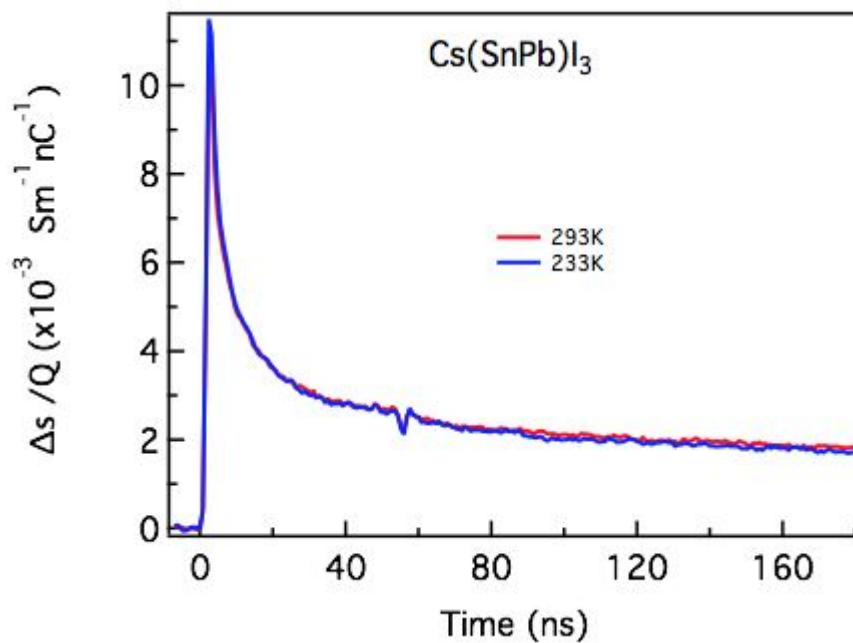


Figure S 11. Charge carrier lifetime of the 3D sample at different temperatures.

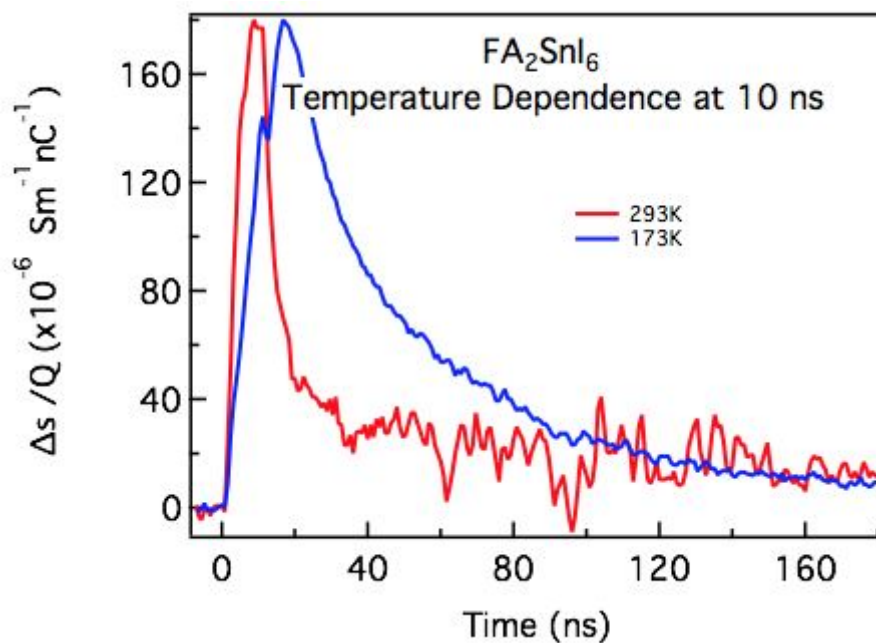


Figure S 12. Charge carrier lifetime of the 0D sample at different temperatures.